sustainability

MDPI

Article

Feasibility Evaluation of Replacing River Sand with Copper Tailings

Liyun Cui [1], Liang Wang [1,2,*], Ying Xu [1], Xing Lou [1] and Hao Wang [1]

[1] School of Civil Engineering and Architecture, Anhui University of Science and Technology, Huainan 232001, China; Cuily@aust.edu.cn (L.C.); yxu@aust.edu.cn (Y.X.); 18137619268@163.com (X.L.); 2018200211@aust.edu.cn (H.W.)

[2] Huaibei Mining Co. Ltd., Huaibei 235000, China

* Correspondence: 2018028@aust.edu.cn; Tel.: +86-0554-6668693

Abstract: This study aims to realize the resource regeneration application of copper tailing (as fine aggregates for partial replacement of natural fine aggregates), which avoid environmental pollution due to many landfills of copper tailings. The compressive strength and durability (dry shrinkage and sulfate attack) tests were carried out to evaluate the effect of copper tailings replacement on the performance of mortar. The results show that the mortar with copper tailings has higher compressive strength than the one with natural sand. More than 14% improvement in compressive strength can be achieved by adding copper tailings with no more than 40% replacement level. The dry shrinkage of mortar was increased with the copper tailings due to the increase of micro pores in mortar by using copper tailings. Compared with the mortar with natural sand, the dry shrinkage can be reduced by adding copper tailings with no more than 20% replacement level. The sulfate attack resistance is improved by using copper tailings, when the replacement rate is more than 20%. In fact, the micro-aggregate filler effect of copper tailings effectively refines the pore structure and forms more stable, uniform and fine interface micro pores, which is of vital significance for mortar to resist external forces and sulfate ion erosion. However, copper tailings, as a porous material, have water release characteristics in cement mortar. This characteristic is not conducive to the filler effect, which decreases the filling rate in later hydration, leading to higher porosity of copper tailings mortar. More importantly, mortar can solidify heavy metals in copper tailings, which prevents loss of heavy metal such as Cu, Zn, Sr, Zr, As, Ga due to environmental problems.

Keywords: copper tailings; strength and durability; binary image analysis; solidify heavy metals

Citation: Cui, L.; Wang, L.; Xu, Y.; Lou, X.; Wang, H. Feasibility Evaluation of Replacing River Sand with Copper Tailings. *Sustainability* **2021**, *13*, 7575. https://doi.org/10.3390/su13147575

Academic Editor: Antonio Caggiano

Received: 12 June 2021
Accepted: 1 July 2021
Published: 7 July 2021

1. Introduction

Waste tailings as filler of mortar proved to be a good choice. Ceren Ince [1] revealed that in replacing part of natural river sand with gold mine tailings from the Lefke-Xeros area, the performance (compressive strength, water penetration depth and carbonization depth) of the gold tailings test block is significantly improved due to the pozzolanic activity and filler effect. It is worth noting that the average particle size of gold tailings in Ceren Ince's paper is about 8 μm. SiO_2 + Al_2O_3 + Fe_2O_3 accounted for 79.36%, which is required by the ASTM C618-15 (Standard Specification for Coal Fly Ash and Raw or Calcined Natural Pozzolan for Use in Concrete) [2]. Actually, the majority of waste tailings, such as copper tailings, iron tailings, nickel tailings, etc. do not have the inherent excellent physical and chemical properties of gold mine tailings from the Lefke-Xeros area, but are inert materials with relatively coarse particles, which are more suitable for use as an aggregate replacement [3–8]. Besides, the thing that cannot be ignored is that tailings (copper tailings and iron tailings) usually contain a small amount of soluble heavy metal ions, whether or not these soluble heavy metal ions can be solidified into the mortar test block [9].

The copper tailings used in this paper are waste byproducts from the Tongling Nonferrous Metals Company's beneficiation to refine useful metals. The copper tailings, micron

scale porous materials, have complex chemical composition and severe weathering during long-term stacking. In addition, the erosion of rainwater causes some soluble heavy metals in copper tailings to migrate to rivers and lakes with rainwater, which severely damages the local ecological environment [10–12]. Tongling Nonferrous Metals Company reveals that the secondary reselection of waste copper tailings requires higher technology, gets lower extraction rate of useful metals, and meanwhile introduces more impurity elements, even harmful toxic elements, so the economic and environmental effects are poor. Therefore, copper tailings are usually used as underground filling in mines. However, the annual output of copper tailings is large, and the underground filling space is limited, resulting in the resource utilization rate being very low. The rest of the copper tailings are often directly landfilled. Therefore, the recycling of copper tailings has become an urgent problem. Generally, considering that the main chemical components of copper tailings are metal oxides such as CaO, SiO_2 and Fe_2O_3 (Table 1), which belong to calcium siliceous material, copper tailings replacing natural sand may have very practical application prospects. B. S. Thomas [13] studied the use of waste copper tailings as natural sand in concrete, and found them to have a replacement rate of up to 60% and to exhibit good strength and durability, providing a reference for actual engineering. Mike Otieno [14] evaluated the feasibility of kimberlite tailings as aggregates in concrete, and found that reasonable design of concrete coarse and fine aggregates, pre-wetting kimberlite tailings aggregates and adding additives can effectively reduce the influence of kimberlite tailings on the workability of concrete. Elizabeth J. Lam et al. [15] studied the mechanical properties (bending test and compression test) of copper tailings used as aggregates to prepare cement mortar, to be used as paving stones for abandoned tailings dams. The results found that the mixed part the tailings increase the bending strength of the mortar by 26% and the compressive strength by 80%. Yuxing Zhang [4] used copper tailings as micronized sand to improve the gradation of artificial sand and found that 20% copper tailings can optimize the artificial sand gradation, and improve the segregation of manufactured sand concrete and the long-term strength value, since copper tailings can fill the interface between manufactured sand and cement slurry to refine the pores. However, it will increase the shrinkage of concrete. The use of copper tailings as aggregate has been proven to be feasible. In the research process, people pay more attention to the impact of copper tailings on mechanical properties and durability, and ignore the influence of copper tailings on the gradation and compactness of natural sand or manufactured sand. Microscopically, they ignored the influence of copper tailings on pore structure under cement-based systems.

Table 1. The chemical composition and physical properties of primary copper tailings.

Component	Wt. (%)	Heavy Metal Component	Wt. (%)
SiO_2	35.04	CuO	0.0702
MgO	2.509	ZnO	0.0553
CaO	30.67	SrO	0.023
Al_2O_3	7.66	ZrO_2	0.0116
Fe_2O_3	17.14	As_2O_3	0.0066
K_2O	1.324	Ga_2O_3	0.0044
Na_2O	0.415		
TiO_2	0.439		
CuO	0.0702		
MnO	0.456		
ZnO	0.0553		
SO_3	3.979		

Therefore, this paper first comparatively analyzed the compactness of natural river sand and mixed fine aggregate based on the solid accumulation theory and particle grading parameters. Then, testing compressive strength, dry shrinkage and sulfate attack provide a reference for the practical application of copper tailings. The microscopic aspect mainly uses MIP test and binary image analysis to compare the internal pore structure of cop-

per tailings mortar, especially the binary image analysis visually demonstrates the pore structure characteristics. Importantly, based on the leaching test, it is tested whether the solidification of heavy metals in the copper tailings mortar meets the requirements of ecological regulations. The replacement of natural sand by copper tailings has not only successfully solved the environmental problems caused by random stacking and loss of heavy metals such as Cu, Zn, Sr, Zr, As, Ga. It is also considered a feasible way to solve the shortage of natural sand resources in China.

2. Materials and Methods

2.1. Cement and Primary Copper Tailings

Ordinary Portland cement (P.O 42.5) is produced at the Bagongshan Cement Plant in Huainan City, Anhui Province, China. The copper tailings are from Tongling Nonferrous Metals Company, Tongling City, Anhui Province, China. Table 1 shows the chemical composition and physical properties of the primary copper tailings. Among them, the total content of CaO, SiO_2 and Fe_2O_3 accounts for 82.85%, and the main mineral ingredients are silica, calcium longite, limestone, gypsum, calcium, iron, etc. (Figure 1). Additionally, the native copper tailings contain a small amount of heavy metal elements (Sr, Zr, Ga, Cu, Zn and As).

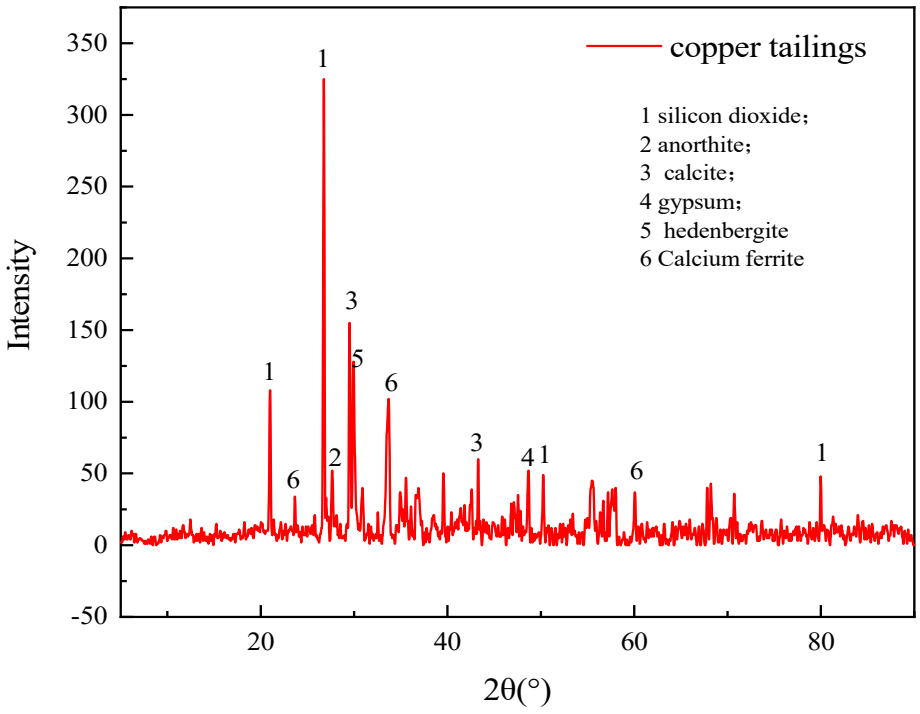

Figure 1. X-ray diffraction spectrum of copper tailings.

The particle size distribution of copper tailings is detected with a laser particle size analyzer, as shown in Figure 2. The median particle size is 110 μm (Figure 2), which belongs to micron particles. The US FEI Inspect F50 field emission scanning electron microscope is used to observe the apparent morphology of copper tailings (Figure 3). It is found that the copper tailings have sharp corner angles and a wide range of particle size distribution.

In addition to the introduction of the physical properties and chemical composition of copper tailings, copper tailings as fine aggregates should also be tested in accordance with JGJ 52-2006 (Standard for technical requirements and test method of sand and crushed stone for ordinary concrete) [16], such as water content (standard method), sludge content (siphon method) and nuclear radiation (radiometer detection) of copper tailings. The results show that the water content of Tongling copper tailings is 26.12%, which is already a high-water content aggregate, and the sludge content of copper tailings is less than 5%, and there is no radiation.

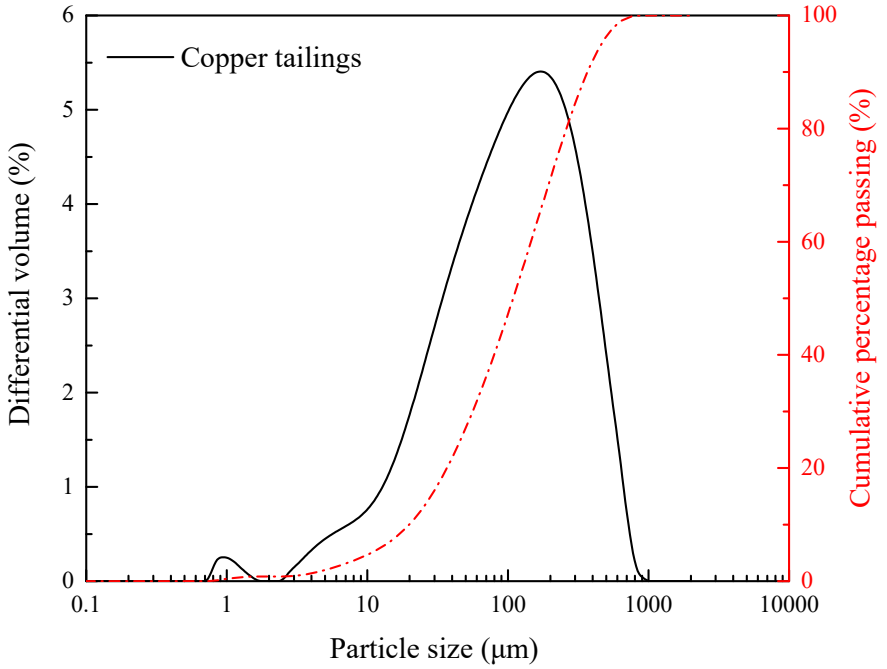

Figure 2. Particle size distribution of copper tailings.

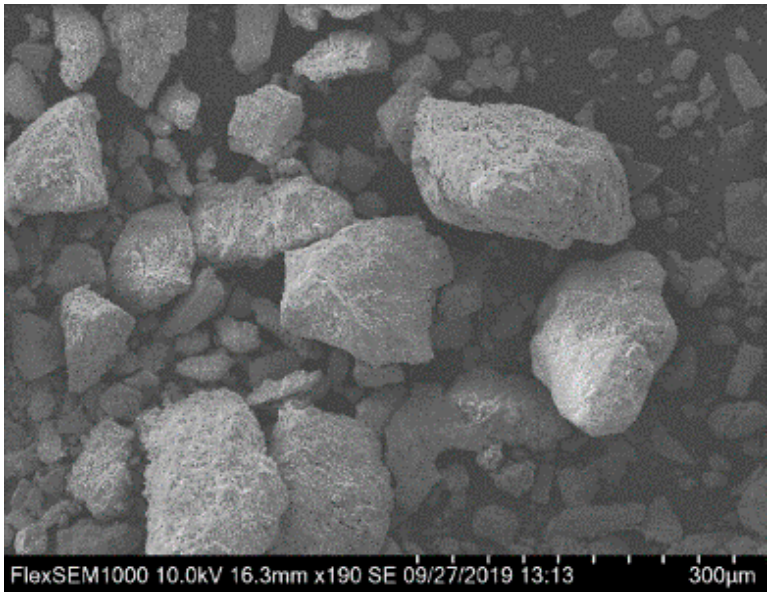

Figure 3. The microscopic morphological characteristics of copper tailings.

The above content mainly tests the basic properties of copper tailings. To study the effect of copper tailings mixed with mortar on performance, the specific mix ratio design of copper tailings mortar (100 g) is designed as shown in Table 2. The numbers T-0% (control group), T-10%, T-20%, T-30% and T-40%, respectively, indicate that the replacement rate of copper tailings is 0%, 10%, 20%, 30% and 40%, and the water-cement ratio is set to 0.55.

2.2. Test Methods

The compressive strength is the most basic parameter index for evaluating the mechanical properties of mortar. In order to obtain a more accurate compressive strength value, the preparation process of the test block needs to be standardized. The steps of test block preparation are as follows. First, put the copper tailings and natural sand in an oven at 105 ± 5 °C for 8 h, weigh them according to the design of the mix ratio, put them

in a dry mixing pot, and mix them dry at slow speed for 30 s, and mix well. Then, add cement and dry mix for 1 min. Finally, pour all the mixing water into the mixing pot and wet mix for 2 ± 0.5 min. Subsequently, quickly place the freshly mixed mortar in a cube mold (5 cm × 5 cm × 5 cm), place it on a vibrating table for 15 ± 5 s, smooth the surface, and put it in the curing chamber for 24 h before demolding. After that curing for 6 days, 27 days and 89 days, take it out and measure its compressive strength.

Table 2. The basic mix design (100 g).

Serial Number	Cement (g)	Natural River Sand (g)	Copper Tailings (g)	Water (g)
T-0%	28.14	56.31	0	15.49
T-10%	28.14	50.68	5.63	15.49
T-20%	28.14	45.05	11.26	15.49
T-30%	28.14	39.42	16.89	15.49
T-40%	28.14	33.79	22.53	15.49

Dry shrinkage is used to evaluate the shrinkage deformation of mortar specimens, and it is one of the reference indicators of mortar durability. The drying shrinkage experiment in this study based on ASTM C596-2018 (Standard test method for drying shrinkage of mortar containing hydraulic cement) [17] prepare cuboid specimens with size of 25 mm × 25 mm × 280 mm for testing the shrinkage properties of copper tailings mortar. During the experiment, the curing temperature is 20 ± 3 °C and the curing humidity is 50 ± 5%.

Sulfate attack [18] requires that the cube mortar (50 mm × 50 mm × 50 mm) be cured in water bath for 28 days, and then completely immersed in 5% sodium sulfate solution (500 g sodium sulfate decahydrate and 3900 g water are mixed evenly). Take out the test block after soaking for 30 days and 120 days. The sodium sulfate solution needs to be replaced every two weeks. The same batch of mortar test blocks were taken out on the 58th and 148th days after being cured in water. The loss of compressive strength indicates the resistance of the mortar to sulfate erosion. Therefore, the compressive strength loss rate (%) is selected as the index [13], and the formula of compressive strength loss rate ΔC is as follows:

$$\Delta C = \frac{(C_w - C_s)}{C_w} \times 100\% \quad (1)$$

Note: C_s means that compressive strength after sulfate attack. C_w represents compressive strength after water curing.

2.3. MIP and SEM

MIP experiment describes a test method for the characteristics of the pore structure inside the mortar. The mercury intrusion device is Autopore IV (9500), the pressure range is set from 0.1 to 61,000 psia, the contact angle is 130°, and the quality of the sample to be tested is controlled between 1.6 g and 2.1 g to prevent the mass of the test block from being too large or too small to affect porosity test results [19]. The surface morphology analysis of the mortar used the electron microscope picture taken by the FEI Inspect F50 field emission scanning electron microscope under the electron beam acceleration voltage 20.00 kV.

2.4. Leaching Experiment

Copper tailings containing heavy metal elements are used as fine aggregates of mortar, and we should conduct leaching experiment on copper tailings mortar to detect whether it is toxic to the environment. The leaching test in this paper was carried out with reference to the British Standard BS EN12457-2002 [20]. First, a wet sample from the tailings mortar specimen was dried and crushed to a particle shape of less than 2 mm. Distilled water is used as the leaching agent for the leaching experiment to eliminate the interference of water ions on the experiment results. Here, the liquid to solid ratio is set to 10:1 (l/kg), and the water bath temperature is set to 20 ± 5 °C, and allowed to stand for 24 h. Next, filter

the large particles with 0.45 μm filter paper, and remove the ultrafine slurry powder that may exist in the filtrate with a centrifuge. The stable pH value of the filtrate was recorded by pH meter at room temperature (20 ± 5 °C). The concentrations of five heavy metal elements (Sr, Zr, Ga, Cu, Zn and As) in the filtrate were determined by inductively coupled plasma emission spectrometer (ICP-OES) [21].

3. Results

3.1. Properties of Mixed Fine Aggregate

3.1.1. Testing the Basic Properties of the Mixed Sand

Figure 4 shows the dried natural sand and copper tailings. It can be seen that the particle size of copper tailings is smaller than that of river sand and the color is darker.

Figure 4. The photos of natural sand (**left**) and copper tailings (**right**).

Refer to JGJ 52-2006 (Standard for technical requirements and test method of sand and crushed stone for ordinary concrete) to test the loose bulk density, close bulk density, and fineness of the mixed fine aggregate (river sand and copper tailings). The results are shown in the Table 3.

Table 3. The physical properties of mixed sand.

Test Items	0%	10%	20%	30%	40%
Loosely packed density (kg/m^3)	1573	1624	1641	1661	1690
Dense packing density (kg/m^3)	1703	1777	1840	1913	1982
Fineness (μf)	2.4	2.15	1.86	1.69	1.51
JGJ5-2006	coarse sand: 3.7~3.1 medium sand: 3.0~2.3 fine sand: 2.2~1.6				

It can be seen that the bulk density and dense packing density of the mixed fine aggregate increase with the increase of the copper tailing content. The fineness decreases with the increase of the copper tailing content. River sand belongs to medium sand, the mixed fine aggregate mixed with 10% to 30% copper tailings in river sand belongs to fine sand, and the mixed fine aggregate mixed with 40% copper tailings in river sand belongs to superfine sand. Therefore, the incorporation of copper tailings greatly reduces the fineness of fine aggregates.

3.1.2. Packing Theory of Solid Particles (Fuller Theory)

It is meaningful for Chao-Lung Hwang to study the packing density of solid particles based on Fuller's curve [22]. Fuller theory is used to optimize the filling ratio. It is to determine the distribution of various particle sizes in the gradation from the perspective of the combination of aggregates in which proportions can achieve the maximum density [22]. The closer the material (fine aggregate) gradation curve is to the parabola (Fuller curve), the higher the degree of compaction. Here is the Fuller general formula of A.N.Talbol:

$$y = 100\left(\frac{x}{D}\right)^n \quad (2)$$

Here, y is theoretical cumulative pass rate (%), x is the particle size, D is the maximum particle size of solid aggregate and n is gradation index.

A.N.Talbol proposes that materials have better density (n = 0.3~0.5). The larger the n, the denser the material system, that is, the tightest packing and the smallest porosity are reached when n = 0.5. However, modern concrete requires a certain degree of fluidity and excessive density will reduce the slump of concrete, so 0.45 is the best value for n. Hence, MATLAB software fit five sets of sample data based on Equation (2), and the gradation index n and the RMSE and R-square of the fitted curve are obtained, as shown in Table 4.

Table 4. The gradation index n of sample T-0%, T-10%, T-20%, T-30% and T-40% and evaluation of fitting accuracy.

Serial Number	Gradation Index	Evaluation of Fitting Accuracy	
	n	**R-Square**	**RMSE**
T-0%	0.289	0.637	0.275
T-10%	0.328	0.740	0.219
T-20%	0.321	0.771	0.196
T-30%	0.347	0.817	0.171
T-40%	0.369	0.856	0.145

The result reveals that the gradation index of the T-0% is less than 0.3, while the gradation index values of T-10%, T-20%, T-30% and T-40% are all greater than 0.3. With the increase of tailings content, the gradation index shows an overall increasing trend, which shows that the density of the mixed fine aggregate mixed with copper tailings is indeed greater than that of river sand. Besides, the smaller the RMSE and the larger the R-square of the fitted curve, the higher the fitting accuracy, namely, the more suitable the fitting using Equation (2). In Table 4, the continuous incorporation of copper tailings makes the fitting precision of the sand gradation curve higher and higher, and the sample T-40% has the highest fitting degree.

Next, MATLAB software is used to draw the particle gradation diagram and Fuller curve (n = 0.45) of T-0%, T-10%, T-20%, T-30% and T-40% mixed fine aggregates, as shown in Figure 5. It was found that the incorporation of copper tailings mainly increased the number of particles in a small interval around 0.15 mm. With the increase of the amount of copper tailings, the gradation curve of the mixed fine aggregate becomes closer to the ideal Fuller curve (n = 0.45) with the increase of the copper tailings.

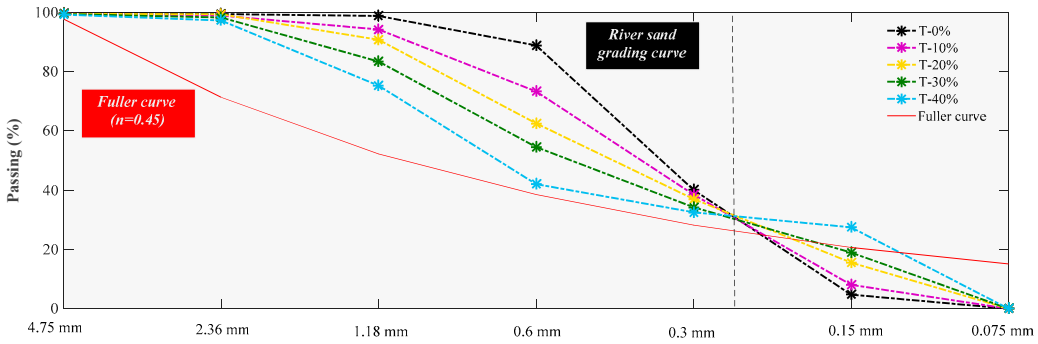

Figure 5. Sample T-0%, T-10%, T-20%, T-30% and T-40% particle gradation map and ideal Fuller curve (n = 0.45).

3.1.3. Characteristics Analysis of Mixed Sand Gradation

The characteristic analysis parameters of the mixed sand are the non-uniformity coefficient C_u and the curvature coefficient C_c (derived from the index used by soil mechanics to analyze the gradation of soil particles), such as Equations (3) and (4).

$$C_u = \frac{d_{60}}{d_{10}} \quad (3)$$

$$C_c = \frac{(d_{30})^2}{(d_{60} \cdot d_{10})} \quad (4)$$

The C_u is used to describe the degree of unevenness of the soil particles. The larger the C_u, the more uneven and the better the particle gradation. The C_c describes the degree of continuity of the soil particle size. The decrease of C_c indicates absence of larger or smaller particles. In engineering, it is considered that $C_u \geq 5$ and C_c = 1 and 3, which is a well-graded soil.

In the paper, the C_u and C_c of soil particle grading are used to evaluate the aggregate particle grading of T-0%, T-10%, T-20%, T-30% and T-40%. The results are shown in Table 5. Noting that the non-uniformity coefficient C_u increases with the increase of the amount of copper tailings. The C_u of T-30% and T-40% are greater than 5, and the C_u of T-20% is close to 5. The C_u of sample T-0% and T- 10% are 2.457 and 3.436 (<5), respectively. This suggests that the incorporation of copper tailings makes the aggregate particles become uneven and the gradation is better. Moreover, the curvature coefficient C_c of T-0%, T-10%, T-20%, T-30% and T-40% fluctuates. Except that the C_c of the T-40% is 0.44, the C_c of T-0%, T-10%, T-20% and T-30% are all in the interval of 0.8~0.95. Therefore, we propose that only the non-uniformity coefficient C_u is considered, the samples T-20%, T-30% and T-40% gradation is better, and only the curvature coefficient C_c is considered, the samples T-0%, T-10%, T- 20% and T-30% are better. Combining these two indicators, the gradation of samples T-20% and T-30% are better than the other three.

Table 5. Sample T-0%, T-10%, T-20%, T-30% and T-40% corresponding gradation index.

Number	Effective Particle Size		Restricted Particle Size	Non-Uniformity Coefficient	Curvature Coefficient
	d_{10} (μm)	d_{30} (μm)	d_{60} (μm)	C_u	C_d
T-0%	0.173	0.26	0.425	2.457	0.919
T-10%	0.163	0.253	0.48	3.436	0.818
T-20%	0.125	0.26	0.57	4.560	0.949
T-30%	0.115	0.26	0.71	6.174	0.828
T-40%	0.1	0.22	0.91	9.100	0.532

3.2. Compressive Strength

Figure 6 shows the compressive strength values and corresponding error bars of T-0%, T-10%, T-20%, T-30% and T-40% in four curing ages (3 days, 7 days, 28 days and 90 days).

It could be seen that the error bar of the test group (90 days) is larger than that of the test group (28 days) error bar. This shows that the copper tailings mortar will increase the strength difference of the same group of test blocks in the later curing. Since the error bar does not exceed 15%, it can be regarded as an effective strength data value.

The compressive strength of control group T-0% and copper tailing mortar (T-10%, T-20%, T-30% and T-40%) increases with the increase of curing age. In the same curing age, the compressive strength of copper tailings mortar is basically higher than that of the control group, and with the increase of the replacement rate of tailings, the strength value has a trend of increasing at first and then decreasing. Figure 6 shows that there is an optimal replacement rate (30%) of river sand replaced by tailing powder. Compared with T-0%, T-30% increased by 17.99%, 16.75%, 14.82% and 14.65% (3 days, 7 days, 28 days and 90 days). During the early curing age (3 days~28 days), T-30% has the highest compressive strength value. The strength of T-20% and T-40% increased obviously during the curing period from 28 days to 90 days, almost catching up with T-30%. All the above data indicate that copper tailings replace part of river sand as fine aggregate of mortar to promote strength in both early strength (3 days~28 days) and later strength (90 days), which is consistent with the results of previous research papers [23,24].

The strength of copper tailing mortar is higher than the control group T-0%, which due to the higher packing density of mixed fine aggregate in copper tailing mortar. Micron

scale copper tailings have a more micro-filling effect than millimeter-level river sand. In addition, the copper tailings particles have distinct edges and corners, and the river sand has a smoother surface after long-term erosion by river water, so the mechanical engagement force between the copper tailings and the cement paste matrix is greater.

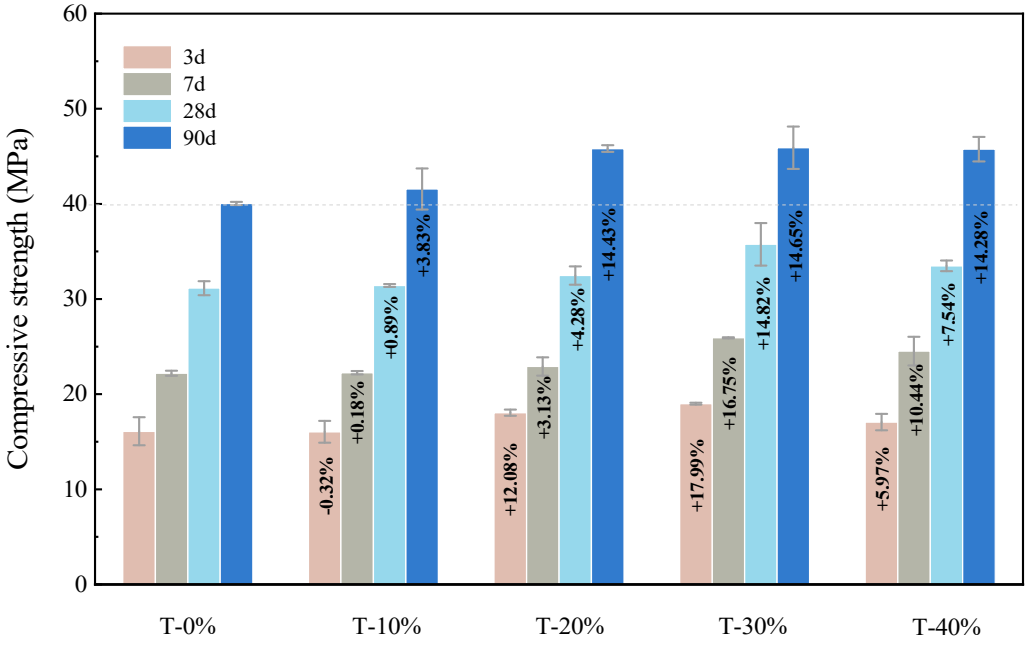

Figure 6. The compressive strength of copper tailings mortar with w/c = 0.55.

3.3. Drying Shrinkage

Drying shrinkage is an important indicator of the durability of cement-based materials. It characterizes the mortar from standard curing conditions (humidity above 95%) to dry curing conditions (low humidity 50 ± 5%), capillary storage of free water evaporation, resulting in the generation of capillary stress, mass decline, volume shrinkage deformation.

Figure 7 shows the shrinkage rate of copper tailings mortar (25 mm × 25 mm × 280 mm) with a water-cement ratio of 0.55 in 90 days. It is obvious that with the increase of copper tailings (10–40%), the shrinkage rate of mortar specimen increases. When the replacement rate of copper tailings is 10–20%, the shrinkage rate is less than T-0%. When the replacement rate of copper tailings is 30–40%, the drying shrinkage rate after stabilization is greater than T-0%. This shows that the addition of 10–20% copper tailings has an inhibitory effect on the shrinkage of the mortar, and overmuch copper tailings (30–40%) will accelerate the shrinkage of the mortar specimens.

Generally, curing of mortar specimens in a low-humidity environment (50 ± 5%) will cause the macro pore water to evaporate in the mortar; nevertheless, the macro pore has little effect on the shrinkage volume. Then there is the evaporation of capillary water (capillary pores are the main influencing factor of volume shrinkage) until all the pore water larger than the critical pore evaporates (the lower the humidity, the smaller the critical pore size); at this time, the volume shrinkage of the mortar is stable [25]. In Figure 7, the dry shrinkage of T-0% on the 21st day of curing was significantly more serious than that of T-10%, T-20% and T-30%. Considering that all mortar specimens in this experiment have the same humidity, the critical pore size is the same. This indicates that after curing for 21 days, T-0% may generate more pores than T-10%, T-20% and T-30%. As the dry curing continues, the capillary pores of T-30% increase and the pores are more refined, so that the drying shrinkage stable period of T-30% is 28% higher than the drying shrinkage rate of T-0%. T-40% has much more capillary pores than T-0% during the whole curing period, so the shrinkage rate of T-40% is much greater than the number of other groups, including T-0%.

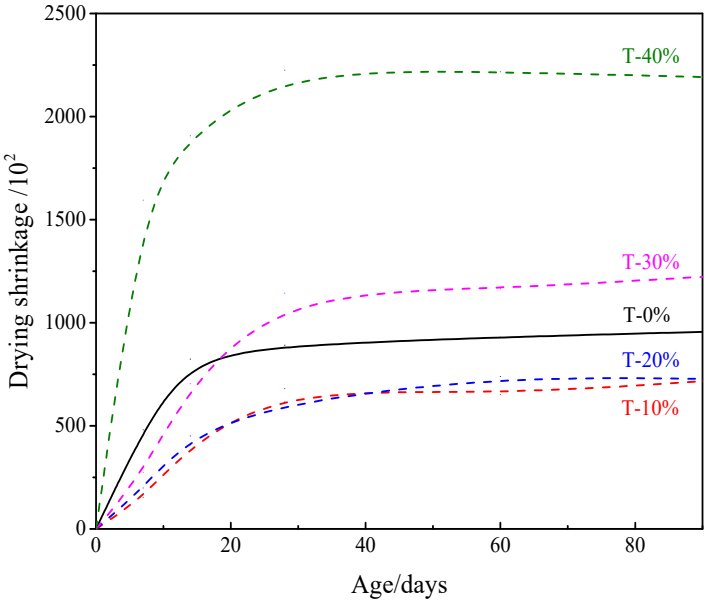

Figure 7. The drying shrinkage of copper tailings mortar for w/c = 0.55.

3.4. Resistance to Sulfate Attack

Sulfate attack is a more dangerous form of deterioration, which is widely present in building structures, and it is another important indicator of durability [26]. Sulfate attack is a complex physical and chemical process. The free SO_4^- in the saturated sulfate solution reacts with the calcium hydroxide in the mortar and the aluminum phase substances in the cement to form expansive substances (expandable gypsum and ettringite), these expansive substances start to fill the internal voids of the mortar and increase the strength of the mortar. This stage is called the compaction stage. With the continuous progress of the chemical reaction, there is no extra space to load expanded gypsum and ettringite. These expandable substances will produce expansion stress on the pore wall. Once the ultimate tensile stress borne by the pore wall is exceeded, the pore structure will be destroyed. The edges and corners of the test block are broken and microcracks are generated, which is called the micro-crack propagation stage. The generation of microcracks provides a transport channel for more sulfate ions to enter the interior of the mortar. These sulfate ions not only consume calcium ions (mainly from calcium hydroxide in the pore solution), but also consume cohesive C-S-H gel, AFm and hydration products containing aluminum phase such as calcium sulfoaluminate hydration. These chemical activities severely damaged the stability of the internal pore structure of the mortar, increased the area of the transition zone between the aggregate and the matrix, and caused a sharp drop in the strength of the mortar. This stage is called the rapid deterioration stage.

Figure 8 shows the appearance of deterioration after five groups of cube mortar specimens (T-0%, T-10%, T-20%, T-30% and T-40%) fully immersed in 5% sodium sulfate solution for 30 days and 120 days. Table 6 gives the strength loss rate after T-0%, T-10%, T-20%, T-30% and T-40% sulfate attack.

It can be seen that after 30 days of full immersion, there are no obvious visible cracks on the surface of all the specimens. With the increase of the replacement rate of copper tailings, there is no obvious rule of the strength loss rate. Except for the decrease in compressive strength of T-20% and T-40%, the compressive strength of other specimen groups increased after sulfate attack (Table 6). This suggests that T-0%, T-10% and T-30% are in the compacting stage, while T-20% and T-40% are in the early stage of micro-crack propagation. It shows that the external sulfate ion has reacted with the calcium-rich hydration product $Ca(OH)_2$ or C-S-H gel on the surface of the specimen to form swelling corrosion products (mainly ettringite and gypsum). There may already be micro-cracks inside to provide a convenient channel for more sulfates to enter [26]. T-10% has obvious

large missing corners and micro-cracks, and the strength loss rate is −12.15%, indicating that T-10% is in the late stage of rapid deterioration. The surface of T-20% has part missing corners and the strength loss rate is −7.64%, indicating that T-20% is in the micro-crack propagation stage. Corners of T-30% have slight peeling and the strength loss rate is −2.66%, implying that T-20% is in the early stage of micro-crack propagation. T-40% seems to have no obvious erosion damage and the strength loss rate is 4.16% (minimal loss of strength). The strength value of T-40% immersion for 120 days is still in the rising stage, so it is considered to still be in the compacting stage. It can be seen that there is a correspondence between the apparent deterioration and the strength loss of the copper tailings mortar in Figure 8 and Table 6. Generally, the more severe the surface deterioration, the greater the loss of strength. It is concluded that with the increase of copper tailings, the resistance to sulfate attack is enhanced. The main reason is that the filler effect of micron scale copper tailings optimizes the internal pore structure of the mortar and effectively prevents the input of sulfate ions.

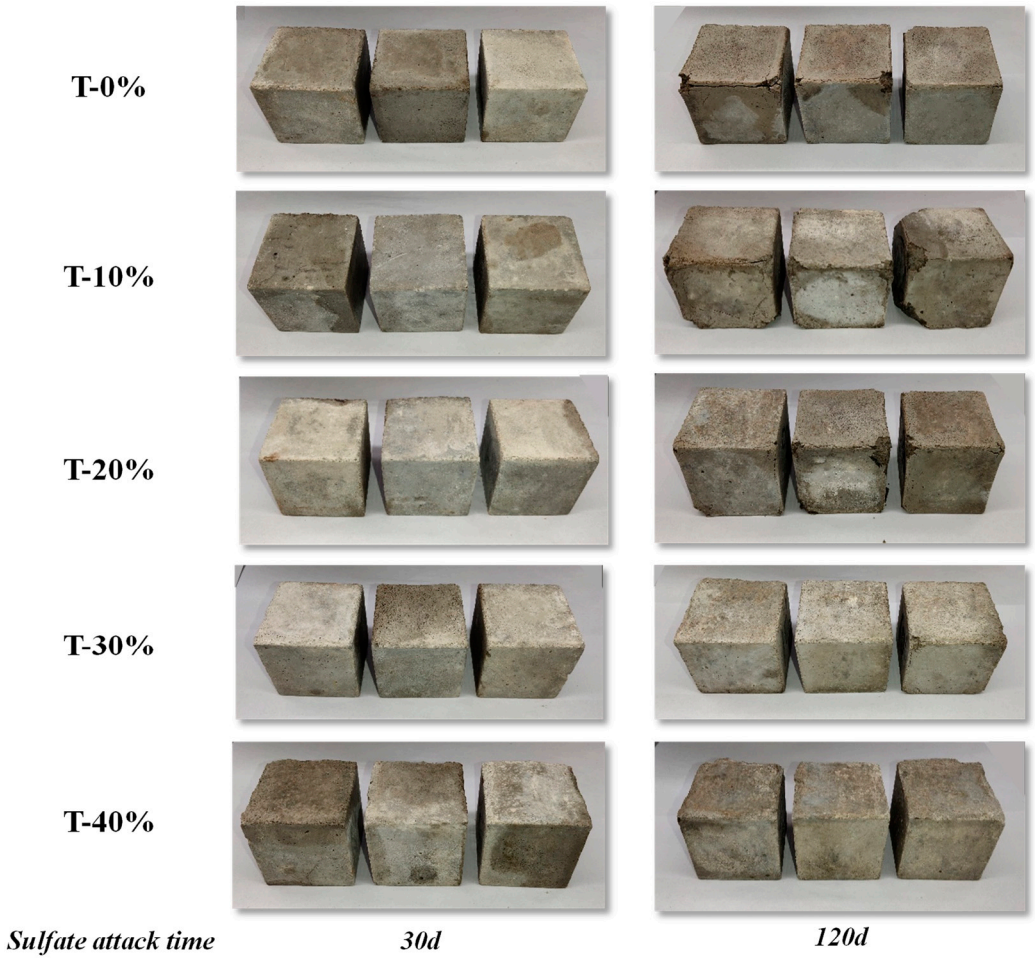

Figure 8. Surface damage of test blocks after 30 days and 120 days of sulfate attack.

Table 6. The strength loss rate of sulfate attack (%).

The Attack of Time	T-0%	T-10%	T-20%	T-30%	T-40%
30 days	1.63	8.51	−1.60	6.16	−3.60
120 days	−10.03	−12.15	−7.64	−2.66	4.16

3.5. Pore Structure

3.5.1. MIP

MIP experiment is the most commonly used and reliable method to characterize the internal pore structure of mortar. The pores of the internal structure of the mortar are usually divided into four levels: gel pores (pore size less than 10 nm), transition pores (10~100 nm), capillary pores (100~1000 nm) and macro pores (greater than 1000 nm). The gel pores are mainly the cavities left after the hydration product C-S-H gel is filled, with the smallest pore volume and basically no effect on the strength. Transition pores mainly refer to the unfilled spaces of large-sized hydration products such as calcium hydroxide, ettringite, and agglomerated C-S-H gel. Spaces that are not filled by hydration products and aggregates may be large pores or the transition zone between the slurry and the aggregate interface. Those with a size less than 1000 nm are considered to be capillary pores, and the rest are macro pores. These two types of pores have a direct impact on the strength. In the early stage of cement hydration (curing time <28 days), large pores may be the main factor affecting the strength. Since the mortar has a water-cement ratio of 0.55, there will be larger pores at the initial stage of hydration, and the large pores will be continuously filled in the later stage of cement hydration; the pore structure distribution will move to small pores, and the pore structure will be continuously optimized.

Table 7 gives the pore characteristic parameters of T-0% and T-30% at the curing ages of 7 days, 28 days and 90 days (including total porosity, average pore size, most probable pore size and fractal dimension). The most probable pore size means the pore size corresponding to the largest pore volume. The fractal dimension represents the roughness and complexity of the pore structure. Currently, the larger the fractal dimension, the more complex the internal structure and the rougher the pore surface. Figure 9a–c shows the pore accumulation curve and pore size distribution diagram of T-0% and T-30% at the ages of 7 days, 28 days and 90 days.

Table 7. Pore characteristic parameters of T-0% and T-30% after 7 days, 28 days and 90 days.

	T-0%	**T-30%**	**T-0%**	**T-30%**	**T-0%**	**T-30%**
Curing age (days)	7	7	28	28	90	90
Total porosity (%)	20.51	20.77	18.69	19.30	14.46	16.27
Average pore size (μm)	22.81	21.53	26.64	25.15	15.42	23.30
Most probable pore size (μm)	77.16	40.25	40.25	40.27	26.29	62.56
Fractal dimension	2.968	3.008	2.974	2.989	3.059	2.983

First, Figure 9a shows the pore size distribution (including the cumulative pore size curve and the pore size distribution curve) for T-0% and T-30% ages at seven days. T-30% and T-0% have little difference for pore size range of the gel. The pore volume of T-30% is slightly larger than T-0% for transition pore size range. The pore volume of T-30% is obviously smaller than T-0% for capillary pore and macropore interval. This shows that T-30% increases the transition pores and reduces the number of capillary pores and macropores. The copper tailings in the early hydration stage have obvious micro-aggregate filler effects. The pore parameters of T-0% and T-30%, such as total porosity, average pore size, most probable pore size and fractal dimension are 20.51%, 20.77%, 22.81 nm, 21.53 nm, 77.16 nm, 40.25 nm, 2.968 and 3.008.

The total porosity of T-0% and T-30% are similar. The average pore size and most probable pore size of T-30% are smaller than T-0% and the fractal dimension is larger. This declares that the replacement of river sand with 30% copper tailings did not significantly reduce the total porosity of the mortar. However, a large amount of copper tailings effectively filled the micron-sized pores and increased the roughness of the pore structure.

Figure 9b shows the pore size distribution (including pore cumulative curve and pore distribution curve) of T-0% (28 days) and T-30% (28 days). The cumulative pore size curves of T-0% and T-30% almost coincide with the pore size distribution curves. At this moment, 30% copper tailings seem to have the same effect as 30% river sand. The pore parameters

of T-0% and T-30%, such as total porosity, average pore size, most probable pore size and fractal dimension are 18.69%, 19.30%, 26.64 nm, 25.15 nm, 40.25 nm, 40.27 nm, 2.974 and 2.989 respectively.

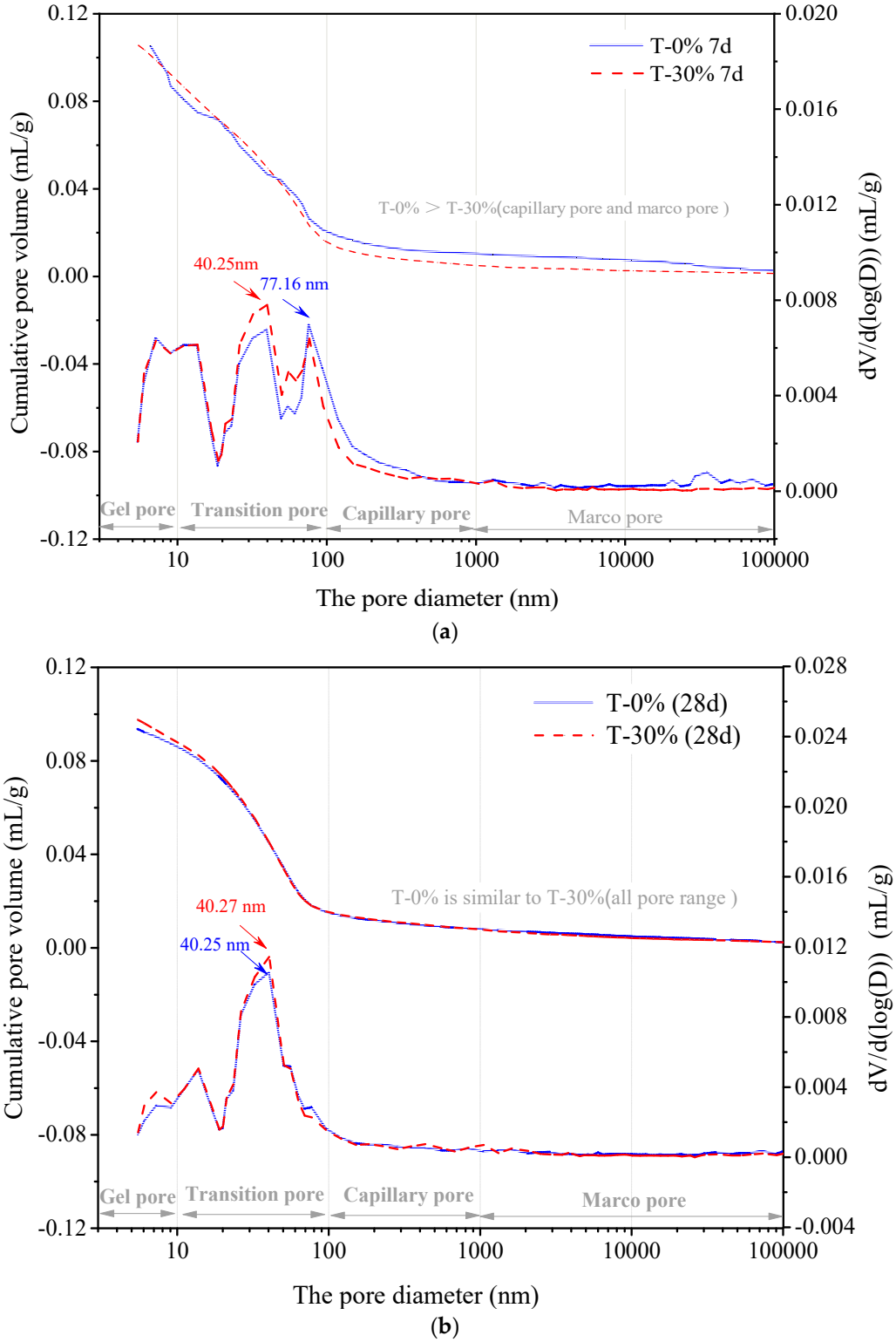

Figure 9. *Cont.*

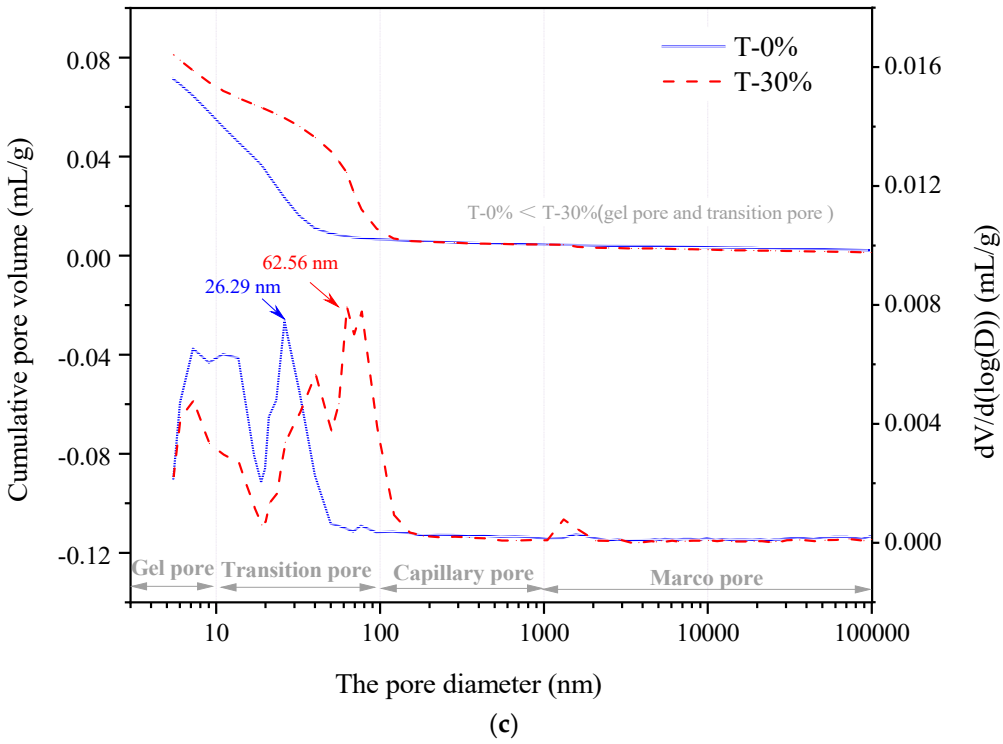

(**c**)

Figure 9. (**a**) The cumulative pore diameter curve of copper tailings (curing for 7 days). (**b**) The cumulative pore diameter curve of copper tailings (curing for 28 days). (**c**) The cumulative pore diameter curve of copper tailings (curing for 90 d).

Compared with T-0%, T-30% has larger total porosity, smaller average pore size and most probable pore size, and larger fractal dimension. This shows that the replacement of river sand with 30% copper tailings will increase the total pores at the age of 28 days, but still has the effect of refining the pore size, and the complexity of the internal pore space becomes more obvious.

Figure 9c gives pore size distribution (including pore cumulative curve and pore distribution curve) of T-0% (90 days) and T-30% (90 days). The pore accumulation curves of T-0% and T-30% in the intervals of capillary pores and macro pores basically coincide, but in the gel pores and transition pores interval, the pore volume of T-30% is obviously larger than that of T-0%. The pore parameters of T-0% and T-30%, such as total porosity, average pore size and most probable pore size are 14.46%, 16.27%, 15.42 nm, 23.30 nm, 26.29 nm, 62.56 nm, 3.059 and 2.983, respectively.

It can be seen that the total porosity of T-30% is higher than T-0% when the hydration age reaches 90 days, the average pore size and the most probable pore size are both larger, and the fractal dimension is smaller. The pore structure of T-30% is looser. It is worth noting that the fractal dimension of T-0% increases with the increase of the curing age, indicating that the increase of hydration products causes the internal structure to be denser and rougher. However, the fractal dimension of T-30% decreases with the increase of curing age. At the initial hydration stage (seven days), the hydration product C-S-H gel is too small to encapsulate the sharp copper tailings, leading to the increase of internal pore structure roughness. Therefore, the fractal dimension of T-30% (seven days) is greater than T-0%. With the continuous hydration, the products are constantly generated to fill and smooth the edges and corners of copper tailings, so the fractal dimension decreases and is lower than T-0%. Accordingly, the sharp edges and corners of copper tailings can effectively increase the pore structure roughness in addition to mechanical bite force.

3.5.2. Binary Image Analysis Based on SEM

In fact, although the MIP experiment is a common test method for studying mortar pores, its results are not intuitive enough to express the pore structure. It is impossible to calculate closed pores and there will still be measurement errors for non-cylindrical pores and ink bottle-shaped pores [27]. Here, this article attempts to use Image-pro software to make binary images of SEM pictures with the gray value threshold value [28], visually and clearly observe the pore characteristics of the micro-section of the mortar, and quantitatively count the number of pores, the maximum area and the area ratio, and combing with the MIP results to analyze the effects of T-0% and T-30% pore structure on the mortar strength, shrinkage and sulfate attack resistance. This analysis is based on the fact that substances with different densities in the electron microscope images correspond to different gray values. For example, the pores with the smallest density appear black, while the unhydrated cement particles with higher density appear bright white [29].

Figure 10a,b show the surface morphologies of T-0% (7 days) and T-30% (7 days), respectively. In Figure 10a, needle-like ettringite and granular C-S-H can be observed cross-stacked, and there are obvious holes (original SEM image). In Figure 10b, the granular C-S-H is filled with some net-like C-S-H, and the surface looks denser (original SEM image). Then, comparing the binary images after Image-pro software processing, it is found that the pore distribution of T-30% (seven days) is more uniform and the interface micro-cracks are narrower.

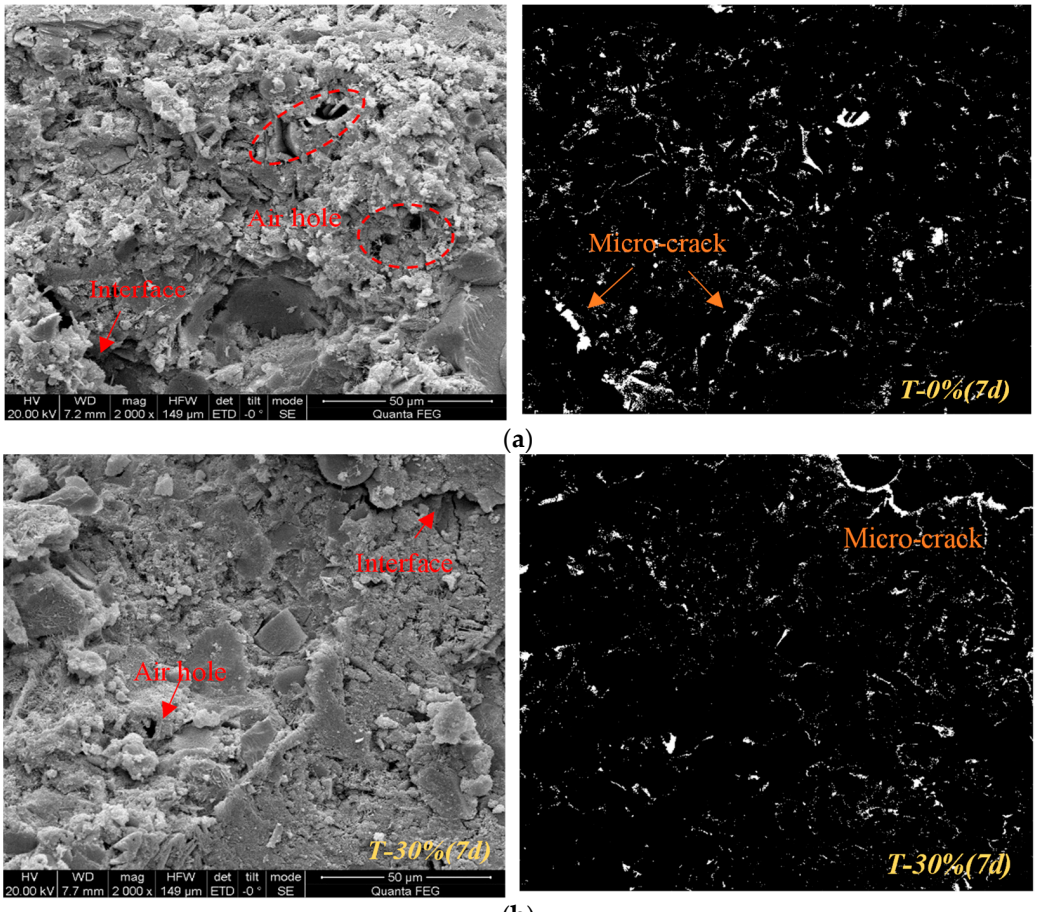

Figure 10. (**a**) The original SEM image and binary image of T-0% (curing for 7 days). (**b**) The original SEM image and binary image of T-30% (curing for 7 days).

Figure 11a,b show the surface morphologies of samples T-0% (28 days) and T-30% (28 days), respectively. The micro section of T-0% (28 days) has no obvious interface area,

but there are obvious large pores. T-30% (28 days) has aggregate interface area and tiny pores. After Image-pro software is processed, the binary image can more clearly capture the micro-interfaces and pores. Similar to the conclusion in the previous paragraph, compared with T-0% (28 days), T-30% (28 days) has more pores (white dots) and a larger interface area, but the pores in other areas are more refined.

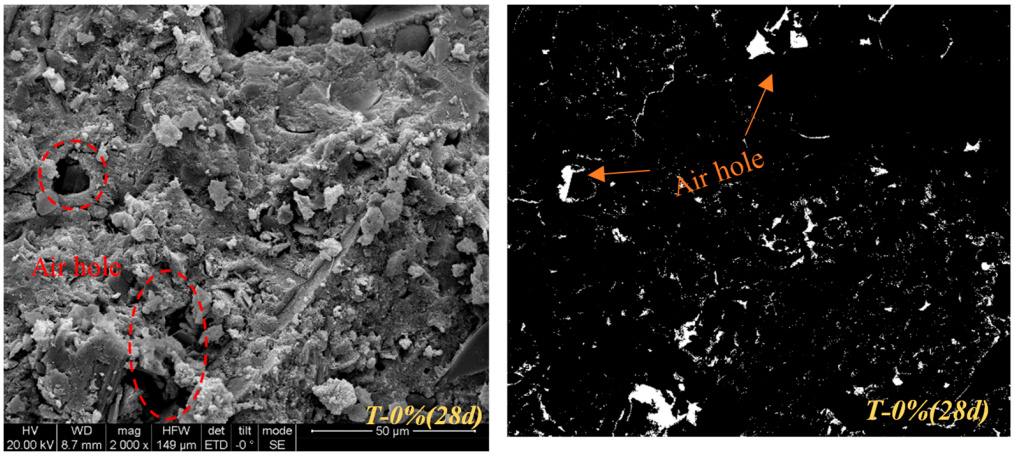

(**a**)

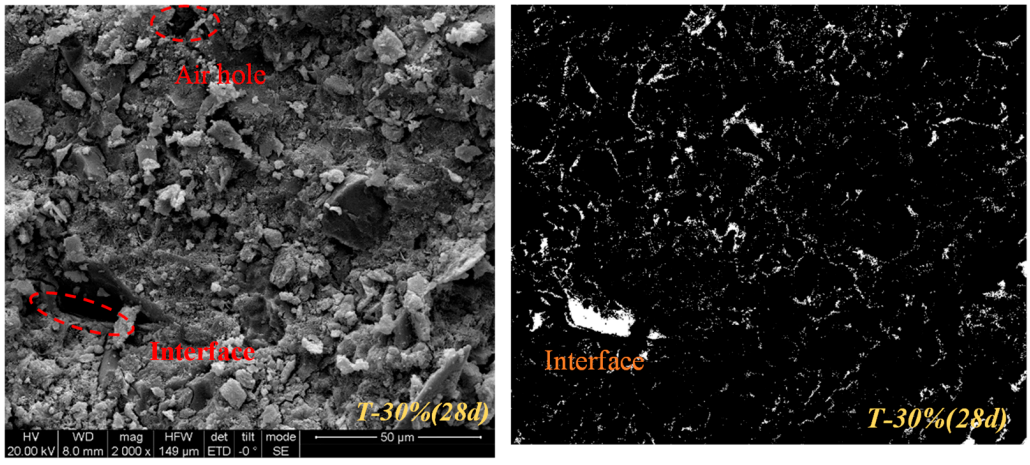

(**b**)

Figure 11. (**a**) The original SEM image and binary image of T-0% (curing for 28 days). (**b**) The original SEM image and binary image of T-30% (curing for 28 days).

Figure 12a,b show the surface morphologies of the samples T-0% (90 days) and T-30% (90 days), respectively. The T-0% (90 days) micro-section aggregate part is tightly wrapped by dense hydration products; there are still obvious small pores, and the overall pore structure is relatively dense. The micro section of T-30% (90 days) looks relatively loose, and the interface transition zone and small pores still exist. The binary image shows that the number of T-30% (90 days) pores (white dots) is obviously more than that of T-0% (90 days). After 90 days of curing, with the continuous generation of hydration products, the large pores of T-0% (28 days) in the medium are filled with hydration products into small pores or directly filled densely. And T-30% still has more micro pores.

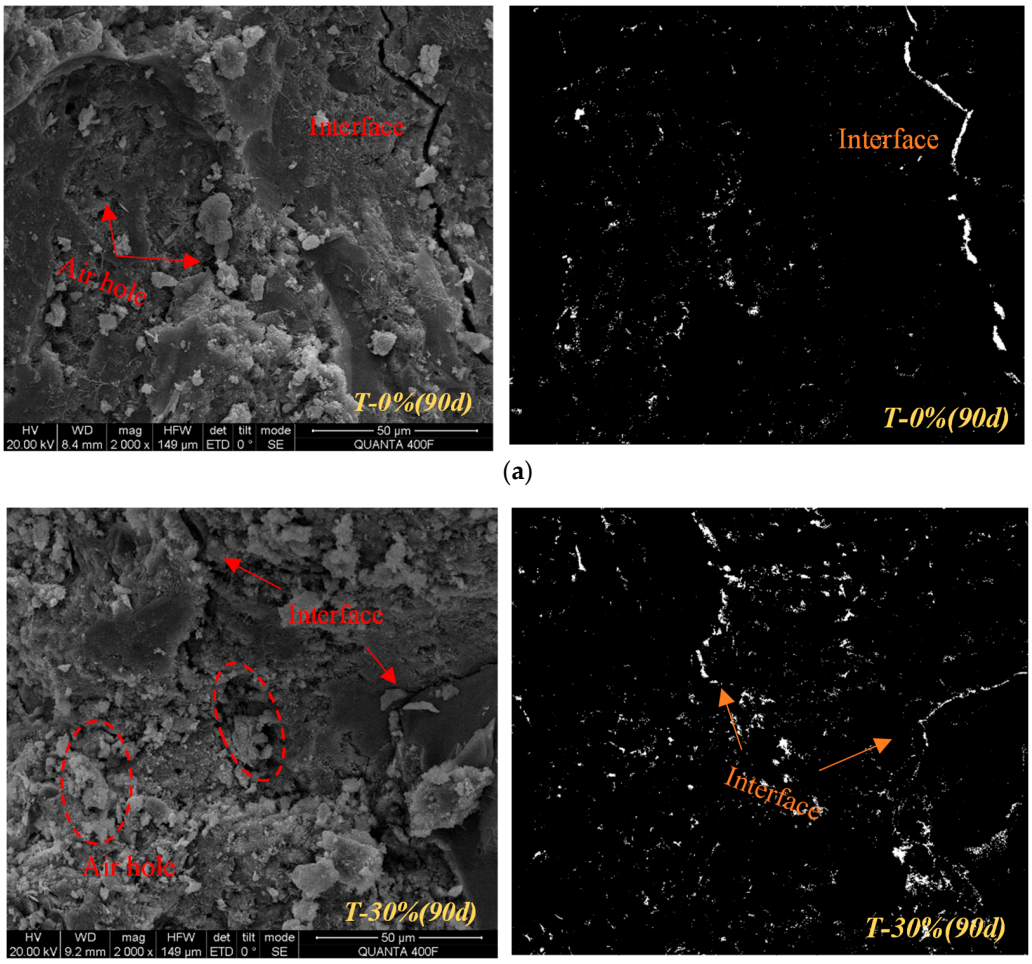

Figure 12. (**a**) The original SEM image and binary image of T-0% (curing for 90 days). (**b**) The original SEM image and binary image of T-30% (curing for 90 d).

Table 8 shows the pore parameters of the mortar micro-section in the binary image, the pores of T-0% (seven days) and T-30% (seven days), such as pore number, average area and area ratio are 5010, 4810, 7.19 μm^2, 5.53 μm^2, 4.05% and 2.95%, respectively. Compared with T-0% (seven days), the micro section of T-30% (seven days) has fewer number of pores, and the average area and area ratio are smaller. MIP experiment reveals that the total porosity and fractal dimension of T-30% are slightly larger than T-0%, and the average pore size and the most probable pore size are smaller. Although the conclusions are slightly different, the binary image analysis is more intuitive (pictures and statistical results), indicating that the 30% copper tailings instead of river sand can effectively refine the pores in the early stage of hydration (seven days). The reasons for the optimization of the pore structure: (1) Copper tailings are used as fine aggregates, and the gradation curve is closer to the Fuller ideal curve, the mixed aggregate gradation is better and the compactness becomes larger (provided in Section 3.1). (2) The micron scale of copper tailings becomes an excellent filler, effectively filling the micro pores of the mortar (micro aggregate effect).

Table 8. The pore parameters (white area) of the micro-section of the binary image.

	T-0%	T-30%	T-0%	T-30%	T-0%	T-30%
Curing age (days)	7	7	28	28	90	90
Number	5010	4810	4363	7349	2438	3602
Average area (μm^2)	7.19	5.53	7.90	5.65	4.74	5.64
Total area of pores (μm^2) ($\times 10^4$)	3.60	2.66	3.45	4.15	1.16	2.03
Total area (μm^2) ($\times 10^5$)	8.93	9.02	8.95	8.89	9.02	9.02
Area ratio (%)	4.05	2.95	3.86	4.67	1.28	2.25
Area ratio based on MIP (%)	20.51	20.77	18.69	19.30	14.46	16.27
Binary image	Figure 10a	Figure 10b	Figure 11a	Figure 11b	Figure 12a	Figure 12b

The pore number, average area and area ratio of T-0% (28 days) and T-30% (28 days) are 4363, 7349, 7.90 μm^2, 5.65 μm^2, and 3.86%, 4.67%, respectively. Compared with T-0% (28 days), T-30% (28 days) has more pores and a larger pore area ratio, but the average area is smaller. The MIP experiment suggests that the total porosity of T-30% (28 days) is higher than that of T-0% (28 days), the average pore size is slightly smaller, the fractal dimension is larger and the pore size distribution is similar (Figure 9b) [4]. The MIP experiment concluded that the pore structure of T-30% is relatively loose. However, the binary image analysis provides the image basis that T-30% has more micro pores and more uniform pore distribution. In addition to the reasons for (1) and (2) in the previous section, this pore feature is also due to the release of water from the copper tailings, which makes a water film around the copper tailings aggregate. This behavior dilutes the water-cement ratio of the interface slurry, resulting in a weakening of the interface between the copper tailings and the cement paste matrix. Compared with micron scale copper tailings, the millimeter size of river sand magnifies the interface damage effect, and it is easier to form large-scale cracks around the river sand (Figure 11a). Although the interface adhesion of copper tailings is poor, the stable and uniform small pore structure (Figure 11b and Table 8) is not prone to damage caused by stress concentration when subjected to external pressure, so T-30% strength is higher. However, the total porosity of T-30% (28 days) is large, and the increase of capillary pores makes the mortar specimen shrink more obviously (Figure 7). Therefore, this more interfacial small pore structure (diluted water-cement ratio) has a lower concentration of $Ca(OH)_2$ solution. The hydration product C-S-H is looser, which provides more space for the conversion of sulfate ions into interface ettringite and reduces the damage to the original pore structure. In addition, the lower calcium ion pore solution at the interface between the tailings powder and the cement paste also hinders the recrystallization process of the interface ettringite and weakens the expansion and failure of the recrystallization pressure of the interface pores (Figure 8 and Table 6).

The pore number, average area and area ratio of T-0% (90 days) and T-30% (90 days) white areas (representing pores) are 2438, 3602, 4.737 μm^2, 5.64 μm^2, 1.28% and 2.25%, respectively. Compared with T-0% (28 days), T-30% (28 days) has more pore numbers and larger average area and area ratio than T-0% (90 days). It shows that adding 30% copper tailings reduces the filling rate of hydration products in the later stage. The water-release stage reduces the alkalinity of the pore solution and forms loose C-S-H around the copper tailings. Moreover, locally high water-cement ratio makes more interface micro pores difficult to be filled (Figure 12b), and the later hydration filling rate decreases. The growth of the compressive strength becomes slower, although it is higher than the control group (T-0%). The shrinkage deformation of T-0% is basically stable at 14 days, while T-30% is stable at 28 days and slightly higher than T-0%. The decrease of the filling rate makes the pore space larger, carries more sulfate-eroded swelling substances, and alleviates the physical expansion effect of 5% sulfate full erosion, which is similar to the explanation in the previous paragraph.

3.6. Leaching Test

To detect the environmental hazard of copper tailings mortar, this paper conducted a leaching test on the T-30% (curing for 28 days and 90 days) and recorded the pH of the leaching solution and the leaching concentration of heavy metals. The leaching test in this paper was carried out with reference to the British Standard BS EN12457-2002 [20]. The leaching agent was distilled water, the s/L ratio was 1:10 (l/kg), and the stirring mode was standing for 24 h.

Table 9 shows the pH of the T-0% and T-30% leaches. T-30% (curing age 28 days and 90 days) has almost no effect on the pH of the leach.

Table 9. The PH and temperature of T-0% and T-30% leaches.

Indexes	T-0%	T-30%	T-0%	T-30%
	PH	Temperature	PH	Temperature
T-0%	12.2	23.7	12.3	23.0
T-30%	12.3	22.9	12.3	23.0

What is important is that ICP-OES is used to detect heavy metal elements in the T-30% (28 days and 90 days curing) leaching solution. The results are shown in Table 10. Group 1 uses XRF to detect six heavy metal elements Sr (19.452), Zr (8.567), Ga (3.270), Cu (56.100), Zn (44.400) and As (4.998) mg/g in copper tailings. It can be seen that the content of Sr, Cu and Zn is higher. If copper tailings as fine aggregate mixed into mortar, T-30% (28 days) in group 2 can only solidify four heavy metal elements (Ga, Cu, Zn and As), and the Sr and Zr elements in the leaching solution are still out of standard state. The six heavy metals in the T-30% (90 days) leachate of group 3 basically meet the environmental quality standard limit. This indicates that copper tailings mortar T-30% has an obvious curing effect on heavy metals in the late curing, and Sr and Zr elements are not cured in the early curing. Therefore, the environmental hazards caused by the loss of heavy metals from copper tailings mortar should not be ignored in actual projects, and the maintenance work of moisture-proof and leaching prevention of copper tailings should be strengthened [30].

Table 10. The concentration of heavy metal elements in T-30% leaching solution.

Heavy Element	Group 1 (mg/g)	Group 2 (mg/L)	Group 3 (mg/L)	Standard 1	Standard 2
	XRF Result	Mortar for 28 Days	Mortar for 90 Days		
Sr	19.452	32	0.543	-	-
Zr	8.567	1.18	-	-	-
Ga	3.270	0.001468	0.000872	-	-
Cu	56.100	0.005075	0.392	≤1 mg/L	5
Zn	44.400	0	-	≤2 mg/L	0.1
As	4.998	0.000245	0.000512	≤0.1 mg/L	5

4. Conclusions

This paper attempted to replace natural sand with copper tailings, studied the properties of mixed fine aggregates and the performance and microstructure of copper tailings mortar, and obtained the following conclusions.

- The characteristics of mixed fine aggregates were discussed, and it was found that the incorporation of copper tailings mainly increased the number of particles in a small interval near 0.15 mm, making the gradation curve closer to the ideal Fuller curve (n = 0.45), optimized river sand with poor gradation, and its compactness is increased.
- The compressive strength of copper tailings mortar is basically higher than that of the control group T-0% in the 7–90 days curing age, especially T-30%. The shrinkage rate and the sulfate attack resistance increases with the increase of copper tailings.

- The conclusion of binary image analysis is similar to the results of MIP experiment. However, the binary image can more clearly and intuitively express that T-30% have more, smaller, denser, more complex pores. The micro-aggregate effect (account for micron scale) is more obvious in the early stage of hydration, and the decrease of the hydration filling rate (reason for water release) in the later curing.
- This paper verifies the environmental friendliness of copper tailings mortar through leaching tests. However, environmental pollution caused by the loss of heavy metals in the early stage (28 days) of copper tailings mortar maintenance should be avoided.

Author Contributions: Conceptualization, L.C. and L.W.; software, L.C.; formal analysis, Y.X.; investigation, X.L.; writing—original draft preparation, L.C.; writing—review and editing, L.C., L.W. and H.W.; visualization, L.C.; supervision, L.C.; project administration, L.W.; funding acquisition, L.W. All authors have read and agreed to the published version of the manuscript.

Funding: This research was funded by the Natural Science Foundation of Anhui Province (2008085QE244), Key Research and Development Project of Anhui Province (201904a07020081). China Postdoctoral Science Foundation, grant number NO. 2020M681988.

Institutional Review Board Statement: Not applicable.

Informed Consent Statement: Not applicable.

Data Availability Statement: Not applicable.

Conflicts of Interest: The authors declare no conflict of interest.

References

1. Ince, C. Reusing gold-mine tailings in cement mortars: Mechanical properties and socio-economic developments for the Lefke-Xeros area of Cyprus. *J. Clean. Prod.* **2019**, *238*, 117871. [CrossRef]
2. American Society for Testing and Materials. *Standard Specification for Coal Fly Ash and Raw or Calcined Natural Pozzolan for Use in Concrete*; ASTM International: West Conshohocken, PA, USA, 2019.
3. Fisonga, M.; Wang, F.; Mutambo, V. Sustainable utilization of copper tailings and tyre-derived aggregates in highway concrete traffic barriers. *Constr. Build. Mater.* **2019**, *216*, 29–39. [CrossRef]
4. Zhang, Y.; Shen, W.; Wu, M.; Shen, B.; Chen, X. Experimental study on the utilization of copper tailing as micronized sand to prepare high performance concrete. *Constr. Build. Mater.* **2020**, *244*, 118312. [CrossRef]
5. Li, X.; Zhang, N.; Yuan, J.; Wang, X.; Zhang, Y. Preparation and microstructural characterization of a novel 3D printable building material composed of copper tailings and iron tailings. *Constr. Build. Mater.* **2020**, *249*, 118779. [CrossRef]
6. Ince, C.; Derogar, S.; Gürkaya, K.; Ball, R.J. Properties, durability and cost efficiency of cement and hydrated lime mortars reusing copper mine tailings of Lefke-Xeros in Cyprus. *Constr. Build. Mater.* **2021**, *268*, 121070. [CrossRef]
7. Argane, R.; Benzaazoua, M.; Hakkou, R.; Bouamrane, A. Reuse of base-metal tailings as aggregates for rendering mortars: Assessment of immobilization performances and environmental behavior. *Constr. Build. Mater.* **2015**, *96*, 296–306. [CrossRef]
8. Shettima, A.U.; Hussin, M.W.; Ahmad, Y.; Mirza, J. Evaluation of iron ore tailings as replacement for fine aggregate in concrete. *Constr. Build. Mater.* **2016**, *120*, 72–79. [CrossRef]
9. Kundu, S.; Aggarwal, A.; Mazumdar, S.; Dutt, K.B. Stabilization characteristics of copper mine tailings through its utilization as a partial substitute for cement in concrete: Preliminary investigations. *Environ. Earth Sci.* **2016**, *75*, 227. [CrossRef]
10. Yang, Y.; Li, Y.; Sun, Q.Y. Archaeal and bacterial communities in acid mine drainage from metal-rich abandoned tailing ponds, Tongling, China. *Trans. Nonferr. Met. Soc. China* **2014**, *24*, 3332–3342. [CrossRef]
11. Jiang, X.; Liu, W.; Xu, H.; Cui, X.; Zheng, B. Characterizations of heavy metal contamination, microbial community, and resistance genes in a tailing of the largest copper mine in China. *Environ. Pollut.* **2021**, *280*, 116947. [CrossRef] [PubMed]
12. Zheng, Q.; Zheng, L.G.; Xia, Y.M. A study of modes of occurrence and pollution characteristics of heavy metals in Shuimuchong tailings of Tongling, Anhui Province. *Acta Petrol. Mineral.* **2018**, *37*, 993–1001.
13. Thomas, B.S.; Damare, A.; Gupta, R.C. Strength and durability characteristics of copper tailing concrete. *Constr. Build. Mater.* **2013**, *48*, 894–900. [CrossRef]
14. Otieno, M.; Ndoro, E. Utilization of kimberlite tailings as aggregates in concrete–strength and selected durability properties. *MRS Adv.* **2020**, *5*, 1259–1266. [CrossRef]
15. Lam, E.J.; Zetola, V.; Ramírez, Y.; Montofré, T.L.; Pereira, F. Making Paving Stones from Copper Mine Tailings as Aggregates. *Int. J. Environ. Res. Public Health* **2020**, *17*, 2448. [CrossRef]
16. *JGJ 52-2006, Standard for Technical Requirements and Test Method of Sand and Crushed Stone for Or-Dinary Concrete*; China Architecture& Building Press: Beijing, China, 2006. Available online: https://www.chinesestandard.net/PDF.aspx/JGJ52-2006 (accessed on 1 April 2021).

17. American Society for Testing and Materials. *ASTM C596-18, Standard Test Method for Drying Shrinkage of Mortar Containing Hydraulic Cement*; ASTM International: West Conshohocken, PA, USA, 2018.
18. Ma, H.; Zhu, H.; Wu, C.; Chen, H.; Liu, J. Study on compressive strength and durability of alkali-activated coal gangue-slag concrete and its mechanism. *Powder Technol.* **2020**, *368*, 112–124. [CrossRef]
19. Liu, S.; Wang, L.; Li, Q.; Song, J. Hydration properties of Portland cement-copper tailing powder composite binder. *Constr. Build. Mater.* **2020**, *251*, 118882. [CrossRef]
20. Akhavan, A.; Golchin, A. Estimation of arsenic leaching from Zn–Pb mine tailings under environmental conditions. *J. Clean. Prod.* **2021**, *295*, 126477. [CrossRef]
21. Hwang, C.L.; Hsieh, S.L. The effect of fly ash/slag on the property of reactive powder mortar designed by using Fuller's ideal curve and error function. *Comput. Concr.* **2007**, *4*, 425–436. [CrossRef]
22. BS EN 12457-1. Characterisation of Waste-Leaching-Compliance Test for Leaching of Granular Waste Materials and Sludges-Part 1: One Stage Batch Test at a Liquid to Solid Ratio of 21/kg for Materials with High Solid Content and with Particle Size below 4 mm (without or with Size Reduction). 2002. Available online: https://shop.bsigroup.com/ProductDetail/?pid=000000000030017786 (accessed on 1 April 2021).
23. Siddique, S.; Jang, J.G. Assessment of molybdenum mine tailings as filler in cement mortar. *J. Build. Eng.* **2020**, *31*, 101322. [CrossRef]
24. Onuaguluchi, O.; Eren, O. Recycling of copper tailings as an additive in cement mortars. *Constr. Build. Mater.* **2012**, *37*, 723–727. [CrossRef]
25. Li, Z.; Liu, J.; Xiao, J.Z.; Zhong, P.; Wang, J. Drying shrinkage of mortar manufactured with recycled fine aggregate at vary initial saturation degree. *Constr. Build. Mater.* **2020**, *264*, 120621. [CrossRef]
26. Yang, Y.; Zhan, B.; Wang, J.; Zhang, Y.; Duan, W. Damage evolution of cement mortar with high volume slag exposed to sulfate attack. *Constr. Build. Mater.* **2020**, *247*, 118626. [CrossRef]
27. Moro, F.; BöHni, H. Ink-Bottle Effect in Mercury Intrusion Porosimetry of Cement-Based Materials. *J. Colloid Interface Sci.* **2002**, *246*, 135–149. [CrossRef] [PubMed]
28. Rani, D.; Rahul, A.V.; Santhanam, M. A multi-analytical approach for pore structure assessment in historic lime mortars. *Constr. Build. Mater.* **2021**, *272*, 121905. [CrossRef]
29. Scrivener, K.L. Backscattered electron imaging of cementitious microstructures: Understanding and quantification. *Cem. Concr. Compos.* **2004**, *26*, 935–945. [CrossRef]
30. Mashifana, T.; Sithole, T. Clean production of sustainable backfill material from waste gold tailings and slag. *J. Clean. Prod.* **2021**, *308*, 127357. [CrossRef]